

# P1AC: Revisiting Absolute Pose From a Single Affine Correspondence

Jonathan Ventura

Department of Computer Science & Software Engineering

California Polytechnic State University

San Luis Obispo, CA 93407 USA

jventu09@calpoly.edu

## Abstract

We introduce a novel solution to the problem of estimating the pose of a calibrated camera given a single observation of an oriented point and an affine correspondence to a reference image. Affine correspondences have traditionally been used to improve feature matching over wide baselines; however, little previous work has considered the use of such correspondences for absolute camera pose computation. The advantage of our approach (P1AC) is that it requires only a single correspondence in the minimal case in comparison to the traditional point-based approach (P3P) which requires at least three points. Our method removes the limiting assumptions made in previous work and provides a general solution that is applicable to large-scale image-based localization. Our evaluation on synthetic data shows that our approach is numerically stable and more robust to point observation noise than P3P. We also evaluate the application of our approach for large-scale image-based localization and demonstrate a practical reduction in the number of iterations and computation time required to robustly localize an image.

## 1 Introduction

Image-based localization is the process of determining the pose of a query image in a reference coordinate system by comparing with pre-registered images in a database. Image-based localization is an important technology for many applications including robotics, self-driving cars and augmented reality. It also forms an essential component of large-scale structure-from-motion pipelines.

The dominant method for image-based localization is to estimate the camera pose from correspondences between 2D features in the query image and known 3D points in the scene. Because these correspondences are likely to contain mismatches, a best-fit model is found through Random Sample Consensus (RANSAC) [15] or one of its derivatives [10, 29], where camera pose hypotheses are estimated from minimal samples of three point correspondences using a perspective-three-point (P3P) algorithm [15, 40].

In cases of very wide-baseline matching or extreme differences in viewing angle, affine-covariant features increase match reliability in comparison to traditional difference-of-Gaussian detectors such as SIFT [32]. A match between affine-covariant features, which we will call an affine correspondence (AC), estimates a  $2 \times 2$  affine transformation matrix between the local regions around the corresponding points in the two images.

Recently, several authors have developed a theory of the constraints induced by ACs on two-view geometry [6, 41, 14], and minimal solvers for relative pose from ACs. However, little attention has been given recently to the topic of absolute pose computation from ACs. We propose to revisit the topic of absolute pose computation from a single AC [25, 18]. In this work we remove limiting assumptions made in previous work and propose the first general solution for absolute pose from a single AC. We call this the perspective-one-affine-correspondence (P1AC) problem. In comparison to P3P, our P1AC solution only requires a single correspondence instead of three

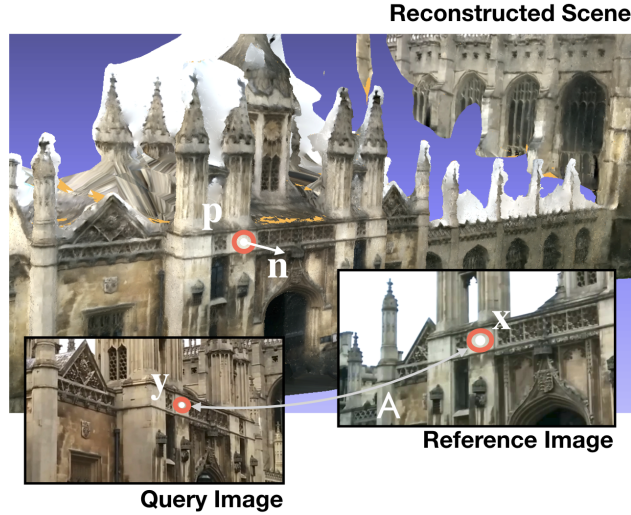


Figure 1: Overview of the P1AC problem. Our goal is to estimate the pose of a query image based on a single 2D observation of a known 3D oriented point in the scene and an affine correspondence to a reference image with known pose.

in the minimal case, and thus reduces sensitivity to point observation noise and the number of iterations required for RANSAC. We demonstrate these advantages through experiments on synthetic and real data.

In the following, we review related work on absolute pose computation and the use of affine correspondences (Section 2), derive our minimal solution for absolute pose from a single affine correspondence (Section 3), describe our evaluation on synthetic and real data comparing our solver with P3P (Section 4) and discuss the results (Section 5), and provide conclusions and directions for future work (Section 6).

## 2 Related work

Affine correspondences are commonly estimated using either frame-to-frame tracking techniques [33, 1] or by affine-covariant region detection [34]. In the case of frame-to-frame tracking, the deformation of a locally planar surface observed by a moving camera is well-modeled by an affine transformation. For affine-covariant regions, an affine transformation describing the shape of the local region around the interest point is estimated [5]. The affine transformation between two regions  $A_i, A_j$  is then found by  $A_j A_i^{-1}$ . Although affine-covariant regions have been shown to improve match reliability in wide-baseline image matching [35], they also are known to be less robust to illumination change [36]. The affine-covariant fitting step also increases the computation time required for feature detection. Recent work explores the application of convolutional neural networks to learn how to more reliably and quickly detect high-quality affine-covariant regions [37].

Given that affine transformations are estimated during the feature matching stage, recent work has examined how these transformations might be used as extra information to improve image-based localization, visual odometry, and structure-from-motion. Köser developed a theory of relationship between homographies and ACs [24], and Bentolila and Francos demonstrated that an AC provides three constraints on the fundamental matrix [6]. Raposo and Barreto re-derived these constraints [41], making them usable for essential matrix estimation using only two ACs instead of five PCs as is normally needed [38]. Eichhardt and Chetverikov extended relative pose estimation using ACs to handle any central camera model [14]. Eichhardt and Barath [13] demonstrated relative pose estimation from a single AC and a depth map estimated by a neural network. Recently, Barath et al. provided recommendations for speeding up RANSAC when using ACs [3], including local feature geometry refinement and uncertainty propagation in RANSAC; these ideas could very well provide a further speedup in our approach.

Absolute pose estimation using ACs has received relatively less attention than relative pose estimation. Algorithms for absolute pose estimation from PCs has a long history, dating back to Grunert’s solution in 1841 [16].

Among many recent P3P solutions [23, 21, 40] the state-of-the-art Lambda Twist method is fast and numerically stable [40].

Collins and Bartoli [11] derived novel constraints and a minimal solution for the absolute pose of a camera given a single 2D-3D correspondence and the homography between the object plane and the query image. In our case, we assume the surface is locally planar but we do not have access to a homography between the object plane and the query image; instead, we are given an affine transformation between a reference image and the query image.

Köser and Koch introduced a solution for absolute pose from a single AC, with the restriction that the reference image is a scaled orthographic image of a planar surface with the surface normal parallel to the optical axis [25]. In our setting, the reference image is instead a perspective image of a locally planar surface in an arbitrary orientation. Their method could be applied in our setting if we rectified the image and then re-computed the affine region in the rectified image; however, this would be expensive as it would need to be done per-feature.

Haug and Jähne developed a solution for absolute pose from a single AC which allows for an arbitrary normal vector [18]. However, they apply a scaled orthographic projection assumption to the affine region in both the reference and query images, which makes the method less accurate when viewing the surface at more extreme angles. Our method does not make a scaled orthographic assumption and thus is not affected by the viewing angle to the surface.

### 3 Minimal solver

**Notation:** We use a sans-serif capital letter  $M$  for a matrix, a bold lower-case letter  $\mathbf{v}$  for a vector, and an italic lower-case letter  $s$  for a scalar. We use subscripts to denote the rows of a matrix ( $\mathbf{r}_1$  is the first row of matrix  $R$ ) and the dimensions of a vector ( $p_1$  is the first element of  $\mathbf{p}$ ). A tilde over a vector indicates a homogeneous version of that vector ( $\tilde{\mathbf{x}} = [x_1 \ x_2 \ 1]^T$ ). A bar over a matrix ( $\bar{P}$ ) denotes the matrix  $P$  rearranged into a vector.

Consider two pinhole cameras observing a scene. We will assume that the two cameras are calibrated (i.e.,  $K = I$ ), the first camera has extrinsics  $[I \mid \mathbf{0}]$ , and the second camera has extrinsics  $[R \mid \mathbf{t}]$ . We will call the first camera the reference camera and the second camera the query camera. Our goal is to estimate the rotation and translation of the query camera. In the general case, where the reference camera is not at the origin, we first transform the world coordinate system to place the reference camera at the origin and then apply the inverse transform to the resulting solution for  $R$  and  $\mathbf{t}$ .

The inputs to the P1AC problem are: corresponding points  $\mathbf{x}$  and  $\mathbf{y}$  in the reference and query image, respectively;  $A$ , the affine transformation from the local region around  $\mathbf{x}$  to the local region around  $\mathbf{y}$ ;  $d$ , the depth of the observed 3D point in the reference image; and  $\mathbf{n}$ , the surface normal at the 3D point in the coordinate system of the reference image.

First we will develop a system of constraints on the pose of the query camera induced by the AC, and then we will describe two solutions to this system.

#### 3.1 Constraints induced by AC on camera pose

Define a function  $f : \mathbb{R}^2 \rightarrow \mathbb{R}^2$  that maps points in the first image to points in the second. Let  $\mathbf{x}, \mathbf{y}$  be corresponding points in the two images such that  $\mathbf{y} = f(\mathbf{x})$ . The first-order approximation of  $f$  centered at  $\mathbf{x}$  is  $\hat{f}(\mathbf{u}) = \mathbf{y} + A(\mathbf{u} - \mathbf{x})$  where  $A = \nabla f(\mathbf{x})$  is the affine transformation matrix.

Let  $\pi^{-1} : \mathbb{R}^2 \rightarrow \mathbb{R}^3$  be the mapping from a point in the first image to the local 3D surface. Then we have

$$f(\mathbf{u}) = \pi(R\pi^{-1}(\mathbf{u}) + \mathbf{t}). \quad (1)$$

The projection function  $\pi(\mathbf{p})$  is straightforward:  $\pi(\mathbf{p}) = [p_1/p_3 \ p_2/p_3]^T$ . The un-projection function  $\pi^{-1}(\mathbf{u})$ , however, requires knowledge of the scene geometry. We assume that the cameras observe a locally planar surface defined by a 3D point  $\mathbf{p} = d\tilde{\mathbf{x}}$  and normal  $\mathbf{n}$  such that  $\mathbf{p}$  projects to  $\mathbf{x}$  and  $\mathbf{y}$  in the first and second cameras,

respectively. Let  $\mathbf{u} = \mathbf{x} + \mathbf{z}$  be a point in the neighborhood of  $\mathbf{x}$ . To determine  $\pi^{-1}(\mathbf{u})$  we will first intersect the ray  $\mathbf{u}$  with the plane to determine its corresponding 3D point. The plane is defined by

$$\mathbf{n}^T(\mathbf{p}' - \mathbf{p}) = 0 \quad (2)$$

where  $\mathbf{p}'$  is a point on the planar surface. Parameterizing the ray-plane intersection by  $\mathbf{p}' = \alpha \tilde{\mathbf{u}}$  we have

$$\mathbf{n}^T(\alpha \tilde{\mathbf{u}} - \mathbf{p}) = 0 \quad (3)$$

thus resulting in

$$\alpha = \frac{\mathbf{n}^T \mathbf{p}}{\mathbf{n}^T \tilde{\mathbf{u}}}. \quad (4)$$

Therefore, under the assumption of a locally planar surface, we have

$$\pi^{-1}(\mathbf{u}) = \frac{\mathbf{n}^T \mathbf{p}}{\mathbf{n}^T \tilde{\mathbf{u}}} \tilde{\mathbf{u}}. \quad (5)$$

Let  $\mathbf{q} = R\pi^{-1}(\mathbf{u}) + \mathbf{t}$ . To compute  $\nabla_{\mathbf{z}} f(\mathbf{u})$ , we first apply the quotient rule to the Jacobian of the projection function  $f(\mathbf{u}) = \pi(\mathbf{q})$  :

$$\nabla_{\mathbf{z}} f(\mathbf{u}) = \nabla_{\mathbf{z}} \pi(\mathbf{q}) \quad (6)$$

$$= \nabla_{\mathbf{z}} \left( \frac{1}{q_3} \begin{bmatrix} q_1 \\ q_2 \end{bmatrix} \right) \quad (7)$$

$$= \frac{1}{q_3^2} \left[ q_3 \left( \nabla_{\mathbf{z}} \begin{bmatrix} q_1 \\ q_2 \end{bmatrix} \right) - \begin{bmatrix} q_1 \\ q_2 \end{bmatrix} (\nabla_{\mathbf{z}} q_3) \right] \quad (8)$$

$$= \frac{1}{q_3} \left[ \nabla_{\mathbf{z}} \begin{bmatrix} q_1 \\ q_2 \end{bmatrix} - \frac{1}{q_3} \begin{bmatrix} q_1 \\ q_2 \end{bmatrix} (\nabla_{\mathbf{z}} q_3) \right] \quad (9)$$

To make the expression linear in  $R, \mathbf{t}$  and simplify the later solution of the system of equations we apply the constraint  $\mathbf{v} = \frac{1}{q_3} \begin{bmatrix} q_1 \\ q_2 \end{bmatrix}$  to obtain

$$\nabla_{\mathbf{z}} f(\mathbf{u}) = \frac{1}{q_3} \left( \nabla_{\mathbf{z}} \begin{bmatrix} q_1 \\ q_2 \end{bmatrix} - \mathbf{v} (\nabla_{\mathbf{z}} q_3) \right). \quad (10)$$

Evaluating this expression at  $\mathbf{z} = \mathbf{0}$  we obtain a final formula for  $J = \nabla_{\mathbf{z}} f(\mathbf{u})|_{\mathbf{z}=\mathbf{0}}$ :

$$J = \frac{1}{m} [d(\mathbf{n}^T \tilde{\mathbf{u}})(R_{1:2,1:2} - \mathbf{v} R_{3,1:2}) + (\mathbf{t}_{1:2} - t_3 \mathbf{v}_{1:2}) \mathbf{n}_{1:2}^T] \quad (11)$$

where  $m = \mathbf{n}^T \tilde{\mathbf{u}}(d(\mathbf{r}_3 \tilde{\mathbf{u}}) + t_3)$ .

We multiply  $m$  on both sides of the constraint  $\mathbf{A} = J$  to cancel out the denominator and make the constraint linear. Our set of constraints to be solved is thus

$$v_1(\mathbf{r}_3 \mathbf{p} + t_3) - v_3(\mathbf{r}_1 \mathbf{p} + t_1) = 0 \quad (12)$$

$$v_2(\mathbf{r}_3 \mathbf{p} + t_3) - v_3(\mathbf{r}_2 \mathbf{p} + t_2) = 0 \quad (13)$$

$$ma_{11} - mj_{11} = 0 \quad (14)$$

$$ma_{12} - mj_{12} = 0 \quad (15)$$

$$ma_{21} - mj_{21} = 0 \quad (16)$$

$$ma_{22} - mj_{22} = 0 \quad (17)$$

where the first two constraints enforce that the 3D point projects to the 2D observation in the query camera, and the remaining constraints enforce that the affine transformation matrix equals the Jacobian matrix derived above.

## 3.2 Minimal solutions

We have six independent constraints on the entries of  $R$  and  $\mathbf{t}$  and six degrees of freedom (three for the rotation and three for the translation). Therefore, we can solve for the absolute pose with a single AC.

### 3.2.1 Nullspace solution

If we parameterize the rotation directly as a  $3 \times 3$  matrix, then we have 12 parameters in  $P = [R \mid \mathbf{t}]$ . We can write the six equations 12–17 as a matrix-vector multiply:

$$M\bar{P} = \mathbf{0}. \quad (18)$$

Let  $B$  be the  $12 \times 6$  nullspace of  $M$ . Any solution, up to scale, for  $\bar{P}$  has the form

$$\bar{P} = B\mathbf{b} \quad (19)$$

where  $\mathbf{b}$  is a vector of six coefficients for the basis vectors in  $B$ . Our goal is to find solutions for  $\mathbf{b}$  that make the rotation matrix orthogonal.

We follow the solution procedure described by Ventura et al. [47]. To remove one parameter and simplify the solution, we fix the last coefficient  $b_6 = 1$ . Let  $\mathbf{r}_1, \mathbf{r}_2, \mathbf{r}_3$  be the rows of  $R$  and  $\mathbf{c}_1, \mathbf{c}_2, \mathbf{c}_3$  be the columns. The following constraints ensure that  $R$  is orthogonal, up to scale:

$$\|\mathbf{r}_1\|^2 - \|\mathbf{r}_2\|^2 = 0 \quad (20)$$

$$\|\mathbf{r}_1\|^2 - \|\mathbf{r}_3\|^2 = 0 \quad (21)$$

$$\|\mathbf{c}_1\|^2 - \|\mathbf{c}_2\|^2 = 0 \quad (22)$$

$$\|\mathbf{c}_1\|^2 - \|\mathbf{c}_3\|^2 = 0 \quad (23)$$

$$\mathbf{r}_1 \cdot \mathbf{r}_2 = 0 \quad (24)$$

$$\mathbf{r}_1 \cdot \mathbf{r}_3 = 0 \quad (25)$$

$$\mathbf{r}_2 \cdot \mathbf{r}_3 = 0 \quad (26)$$

$$\mathbf{c}_1 \cdot \mathbf{c}_2 = 0 \quad (27)$$

$$\mathbf{c}_1 \cdot \mathbf{c}_3 = 0 \quad (28)$$

$$\mathbf{c}_2 \cdot \mathbf{c}_3 = 0 \quad (29)$$

Plugging in Equation 19 to these constraints results in a system of ten quadratic equations in twenty-one monomials with variables  $b_1, \dots, b_5$ . After extracting the roots of this system of equations, for each solution we divide  $\bar{P}$  by  $\|\mathbf{c}_1\|$  and negate  $\bar{P}$  if necessary to ensure that  $\det(R) = 1$ .

This system has eight solutions in general. To find the solutions to this system of equations, we use an automatic solver generator to produce a solver based on the action matrix method [28]. The resulting solver involves elimination of a  $47 \times 55$  template, and eigendecomposition of an  $8 \times 8$  matrix. Prior to these steps, we compute the nullspace of  $M$  using singular value decomposition (SVD).

Directly incorporating the set of constraints on the  $3 \times 3$  matrix into the initial system of equations, instead of first computing the nullspace on the initial equations and solving a system of constraints on the nullvector coefficients, led to a larger elimination template produced by the automatic generator and thus a slower solver.

### 3.2.2 3Q3 solution

An faster solution is found using the Cayley parameterization of the rotation with parameters  $x, y, z$ :

$$R = \frac{1}{s} \begin{bmatrix} 1+x^2-y^2-z^2 & 2(xy-z) & 2(y+xz) \\ 2(xy+z) & 1-x^2-y^2-z^2 & 2(yz-x) \\ 2(xz-y) & 2(x+yz) & 1-x^2-y^2+z^2 \end{bmatrix} \quad (30)$$

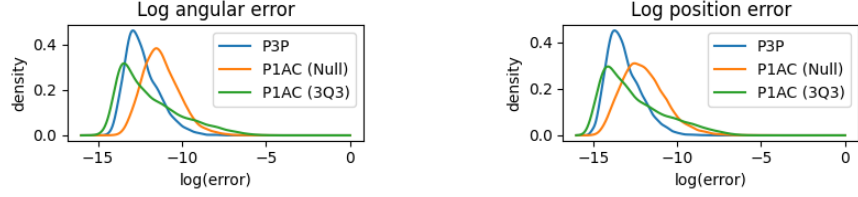


Figure 2: Results of synthetic data experiment with zero noise. The plots are estimates of the underlying distribution produced by Gaussian kernel-density estimation. *Left*: Log angular error; *Right*: Log position error.

where  $s = 1 + x^2 + y^2 + z^2$ . Note that we cannot represent  $180^\circ$  rotations with this parameterization.

After plugging this formulation of  $R$  into the the six equations 12–17, we multiply all equations by  $s$  to cancel out the denominator in  $R$ .

Let  $\mathbf{p} = [st_1, st_2, st_3, x^2, xy, xz, y^2, yz, z^2, x, y, z, 1]^T$ . Writing the equations as a matrix-vector multiply  $M\mathbf{p} = 0$ , we first eliminate  $st$  using Gauss-Jordan elimination. This leaves three quadratic equations in ten monomials on  $x, y, z$  – a 3Q3 problem. Kukulova et al. [26] introduced a fast solver for the 3Q3 problem which produces up to eight solutions for  $x, y, z$ . We used the implementation by Larsson<sup>1</sup> which uses several techniques to improve the stability of the original solver [50]. Once we have obtained solutions for  $x, y, z$ , we solve for  $t$  by backsubstitution into the original equations.

### 3.2.3 Generating points from the AC

As a baseline comparison, we also considered the following solution which uses a standard P3P solver. Let  $A_x$  denote the affine transformation from the canonical frame to the reference image, as returned by the affine region detector. We generate two extra point correspondences  $\mathbf{x}^{(i)} \leftrightarrow \mathbf{y}^{(i)}$  using the formulas

$$\mathbf{x}^{(i)} = \mathbf{x} + A_x \mathbf{b}^{(i)} \quad (31)$$

$$\mathbf{y}^{(i)} = \mathbf{y} + A(\mathbf{x}^{(i)} - \mathbf{x}) \quad (32)$$

where  $\mathbf{b}^{(1)} = [1 \ 0]^T$  and  $\mathbf{b}^{(2)} = [0 \ 1]^T$ . The corresponding 3D points are found by back-projecting onto the plane using Equation 5. We then use the original point correspondence from the AC and the two generated correspondences in a P3P solver to solve for the camera pose.

## 4 Evaluation

We performed evaluations on synthetic and real data to test the numerical stability of our solver, test robustness to various types of noise, and assess its performance as part of a image-based localization system.

We compared the following algorithms in our evaluation:

- **P3P** Standard P3P absolute pose calculation from three 2D-3D point observations. We used the state-of-the-art Lambda Twist P3P solver [40].
- **P3P (1AC)** Lambda Twist P3P solver on PCs generated from a single AC (Section 3.2.3).
- **P1AC (Null)** Our solver using the nullspace solution (Section 3.2.1).
- **P1AC (3Q3)** Our solver using the Cayley rotation parameterization and 3Q3 solver (Section 3.2.2).

In our evaluations we computed two accuracy metrics commonly used in previous work. Given the true camera rotation  $R$  and the estimated camera rotation  $\hat{R}$  we computed the *angular error* as the angle of minimal rotation between  $R$  and  $\hat{R}$ . Given the true camera center  $\mathbf{c}$  and the estimated camera center  $\hat{\mathbf{c}}$ , we computed the *position error* as  $\|\mathbf{c} - \hat{\mathbf{c}}\|$ .

<sup>1</sup><https://github.com/vlarsson/re3q3>



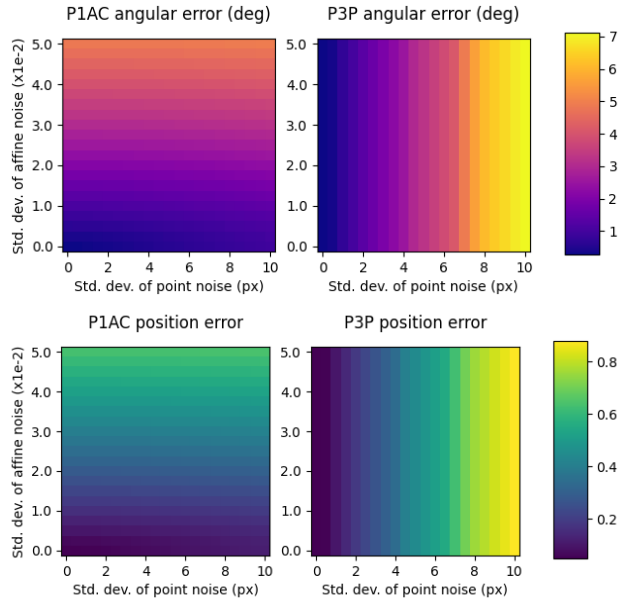


Figure 3: Results of synthetic data experiment with varying levels of point and affine noise.

## 4.1 Synthetic data experiments

We generated synthetic problem instances with varying levels of noise added to the 2D point observations, affine transformations, and normal vectors.

We generated synthetic random problems in the following manner. The first camera has its optical center at the origin  $(0, 0, 0)$  and identity rotation matrix. The second camera has a random rotation and random unit translation. A 3D point is generated by selecting a random 2D point on the image plane in  $[-1, 1] \times [-1, 1]$  and extending it by a random depth in  $[4, 8]$ . The 3D point is then projected to the second camera to produce the second 2D observation. We then calculate the affine transformation from the local homography between the first and second cameras [2].

We add Gaussian noise to the 2D point observations directly. Following Eichhardt et al. [14] we add Gaussian noise directly to the elements of the  $2 \times 2$  affine transformation matrix, although this likely does not model the true noise present in real data. Finally, we add noise to the normal vectors by rotating them by a random rotation whose angle is randomly chosen from a Gaussian distribution. For each problem, a random rotation and translation for the second camera and three affine correspondences between the two cameras are generated and stored in this manner.

### 4.1.1 Numerical stability

To evaluate the numerical stability of each solver, we computed the average angular and position errors of each solver over 10,000 random problem instances with zero noise added. Figure 2 shows the results. The nullspace solver is slightly less accurate than the P3P solver but both have an average error of less than  $1 \times 10^{-10}$ . Interestingly, the 3Q3 solver has the lowest median error, but has a heavier tail because of a few instances where the error was high.

### 4.1.2 Timings

We computed the average timing of the solvers over 10,000 random problem instances. The solvers were implemented in C++ and timings were made on a Macbook Pro with a 2.6 Ghz 6-core Intel Core i7. We used the implementation of Lambda Twist provided in PoseLib [27]. The results are given in Table 1.

Our nullspace solver is about  $45\times$  slower than the P3P solver, but the 3Q3 version is only about  $4\times$  slower.

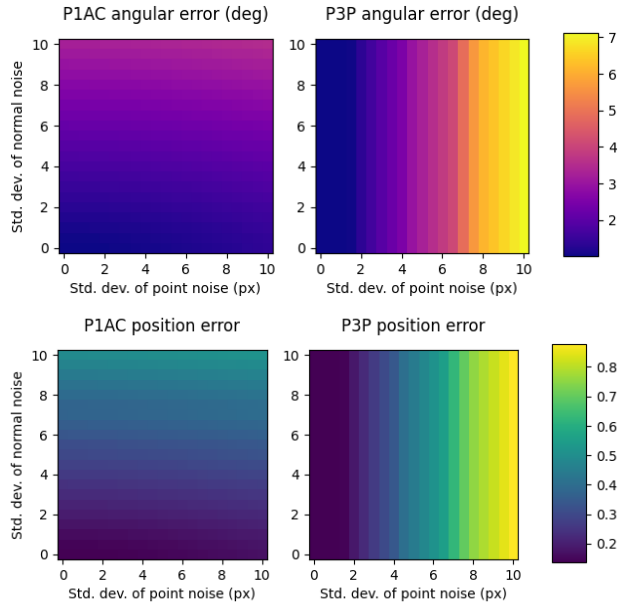


Figure 4: Results of synthetic data experiment with varying levels of point and normal noise.

Method	Time ( $\mu s$ )
P3P [40]	1.18
P1AC (Null)	53.94
P1AC (3Q3)	4.74

Table 1: Average timing in  $\mu s$  over 10,000 trials. Although the nullspace solver is slower than P3P, it reduces overall image localization computation time by reducing the number of RANSAC iterations required (see Section 4.5).

The Lambda Twist solver is based on a careful elimination of the rotation and translation parameters to reveal the underlying elliptic equations in the P3P problem which are solved through diagonalization. Since the nullspace solver involves iterative methods such as SVD and eigendecomposition it is slower than the P3P solver. The 3Q3 version is faster because it does not need to use SVD and it uses Sturm sequences instead of eigendecomposition to solve for the polynomial roots.

### 4.1.3 Noise

We tested P1AC (Null) solver and the P3P solver over a range of noise levels in the 2D point observations, affine transformation matrices, and normal vectors.

Figure 3 presents the results for increasing levels of point and affine noise, with the std. dev. of the normal vector noise set to 1 degree. We increased the std. dev. of 2D observation noise from 0 to 10 pixels and the std. dev. of affine noise from 0 to 0.05.

Figure 4 presents the results for increasing levels of point and normal vector noise, with the std. dev. of the affine noise set to .01. We increased the std. dev. of 2D observation noise from 0 to 10 pixels and the std. dev. of the normal vector noise from 0 to 10 degrees.

The synthetic experiments show that our P1AC solver is affected by 2D observation noise much less than the P3P solver. For low levels of affine and normal noise, the P1AC solver is much more accurate than the P3P solver, even with high 2D observation noise. However, the P1AC solver is affected by affine and normal noise whereas the P3P solver is not. We didn't included results for P1AC (3Q3) here because they are similar to the P1AC (Null) results, except for occasional high errors as mentioned before.



Scene	# Frames		Spatial Extent
	Train	Test	
Great Court	1535	760	$8000m^2$
King’s College	1220	343	$5600m^2$
Old Hospital	895	182	$2000m^2$
Shop Facade	231	103	$875m^2$
St Mary’s Church	1487	530	$4800m^2$
Street	3015	2923	$50000m^2$

Table 2: Dataset summary information for the Cambridge Landmarks dataset [22].

Scene	P3P			P3P (1AC)			P1AC (Null)			P1AC (3Q3)		
	Pos.	Ang.	< 5m/5°	Pos.	Ang.	< 5m/5°	Pos.	Ang.	< 5m/5°	Pos.	Ang.	< 5m/5°
GreatCourt	0.20m	0.14°	85.1%	0.22m	0.15°	83.5%	0.22m	0.15°	83.3%	0.22m	0.15°	83.3%
	0.38m	0.25°		1.51m	1.26°		0.82m	0.65°		0.79m	0.65°	
KingsCollege	0.14m	0.24°	100.0%	0.14m	0.24°	100.0%	0.14m	0.24°	100.0%	0.14m	0.24°	100.0%
	0.22m	0.33°		0.23m	0.33°		0.23m	0.33°		0.23m	0.33°	
OldHospital	0.18m	0.34°	98.9%	0.19m	0.34°	98.9%	0.18m	0.34°	98.9%	0.18m	0.33°	98.9%
	0.32m	0.51°		0.32m	0.52°		0.32m	0.51°		0.32m	0.51°	
ShopFacade	0.07m	0.31°	98.1%	0.06m	0.30°	98.1%	0.07m	0.30°	98.1%	0.07m	0.30°	98.1%
	0.09m	0.48°		0.09m	0.50°		0.09m	0.48°		0.09m	0.48°	
StMarysChurch	0.10m	0.34°	98.9%	0.10m	0.34°	98.9%	0.10m	0.34°	98.9%	0.10m	0.34°	98.9%
	0.15m	0.48°		0.15m	0.48°		0.15m	0.49°		0.15m	0.49°	
Street	0.19m	0.50°	41.1%	0.23m	0.55°	38.0%	0.22m	0.54°	38.6%	0.22m	0.54°	38.7%
	1.34m	1.39°		2.06m	2.79°		1.71m	2.35°		1.68m	2.60°	

Table 3: Error metrics on the Cambridge Landmarks dataset [22]. The median position and angular error for each method is given in the first row for each sequence, as well as the percentage of successfully localized frames. The mean position and angular error is given in the second row for each sequence.

## 4.2 Real data experiments

To evaluate the performance of our method for large-scale image-based localization on real data, we used the benchmark Cambridge Landmarks dataset from Kendall et al. [22]. We chose this dataset rather than other benchmarks commonly used to evaluate feature-based image localization, such as Dubrovnik6k and Rome16k [31], because we needed access to the input images and their ground truth poses whereas most other benchmarks only provide the SIFT descriptors and associated 3D points.

The dataset consists of five scenes with between 231 and 3015 images in each scene. The ground truth pose of each image in each scene was reconstructed using the VisualSFM structure-from-motion software [49, 48] and the images are divided into training and testing sets. In our experiments we used the training images as the reference images with known poses and the test set images as the query images with unknown pose. We only used feature matches between the test images and the training images for computing localization queries and we did not use feature matches between test set images.

We extracted affine covariant features from all images using the VLFeat library [46] using tools from COLMAP [43, 45]. We also create a dense mesh for each scene by first creating a dense point cloud using PatchMatch [4] and then estimating a mesh surface for the point cloud [19]. We used the OpenMVS software package for these steps [9]. To assign a 3D point to each feature point in the training images, we projected the feature point onto the mesh using the ground truth camera pose. The normal vector for the point was then estimated by fitting a plane to

Scene	P3P		P3P (1AC)		P1AC (Null)		P1AC (3Q3)	
	Iter.	Time (ms)	Iter.	Time (ms)	Iter.	Time (ms)	Iter.	Time (ms)
GreatCourt	6 [17]	55 [59]	4 [7]	42 [47]	4 [6]	51 [56]	4 [6]	50 [55]
KingsCollege	5 [5]	70 [74]	4 [4]	59 [59]	4 [4]	62 [62]	4 [4]	60 [60]
OldHospital	8 [11]	62 [66]	5 [5]	52 [52]	5 [5]	52 [55]	5 [5]	52 [55]
ShopFacade	7 [9]	65 [70]	4 [5]	54 [56]	4 [5]	58 [62]	4 [5]	57 [60]
StMarysChurch	5 [5]	59 [63]	3 [4]	52 [55]	3 [4]	61 [61]	3 [4]	60 [61]
Street	18 [272]	40 [51]	10 [59]	20 [31]	9 [36]	23 [35]	8 [38]	22 [33]

Table 4: Median number of iterations and timing on Cambridge Landmarks dataset [22]. The mean is given in square brackets.

the 100 nearest neighbor vertices on the mesh.

### 4.3 Image localization procedure

For each test image, we found a set of candidate image matches from the set of training images in the scene using vocabulary tree search [39] and fast geometric verification [44] as implemented in COLMAP. All feature matches from all related training images were used as input feature correspondences for each test image.

To estimate the pose of each test image using either method, we processed the set of feature correspondences using LO<sup>+</sup>-RANSAC [29] as implemented in RansacLib [42]. We used the EPnP algorithm [30] for local optimization (LO) with a non-minimal set of correspondences. We set the number of LO steps to 10 and the number of least-squares iterations to 10. We performed local optimization from the first iteration, rather than waiting until after 50 iterations as suggested in [29], since the number of iterations required by all methods was low. We found that a relatively large inlier threshold of 16 pixels worked well for both methods. The maximum number of iterations was set to 1000. For least-squares refinement we used Levenberg-Marquardt optimization over the re-projection error of the 3D points.

### 4.4 Pose accuracy

A summary of error metrics on the Cambridge Landmarks dataset is given in Table 3. We report the median and mean position and angular error. We also report the percentage of successfully localized frames, with the success criteria being a position error less than 5m and an angular error less than 5°. For all metrics we excluded cases where the number of inliers was less than 10. In all but the two largest scenes, the median and mean errors for each method was comparable and both methods were able to successfully localize the same number of images. In the two largest scenes (Great Court and Street), the median and mean error for the affine-based methods were slightly higher and the percentages of successful frames were slightly lower than the P3P result. Our P1AC solvers outperformed the baseline P3P (1AC) method in terms of mean error and percentage of frames successfully localized on these sequences.

### 4.5 Timings

Table 4 summarizes the number of iterations and computation time for each method. These timings were recorded on a server with an AMD Epyc 7551P 2.0 GHz CPU and 256 GB RAM. We report the median and mean number of iterations and the median and mean computation time in milliseconds to compute an image localization for each method (not including the time required to compute and match features, which is common to all methods). The affine-based methods required fewer median and mean iterations than P3P on each scene. Our P1AC methods was faster than P3P on five out six scenes. The baseline P3P (1AC) method was faster than our methods, but localized fewer frames successfully as reported above. The P1AC (3Q3) solver was slightly faster than P1AC

(Null). Note that for all methods, local optimization, least-squares regression, and inlier testing dominate the computation time rather than minimal solver, and thus the computation time per iteration is more affected by the number of correspondences than the minimal solver computation time.

## 5 Discussion

Through our experiments on synthetic data, we showed that our P1AC solvers are more robust to point observation noise than the P3P solver. This follows from the fact that P1AC uses only a single point observation where as P3P uses three. However, P1AC is affected by noise in the affine transformation matrix and the normal vector, whereas the P3P solver does not use these inputs and thus is not affected by noise in their estimation.

In terms of timing, our P1AC solvers are slower than the P3P solver. However, all of the solvers are fast (on the order of 1-10 microseconds) and their computation time is negligible compared to other steps in the random sampling process such as local optimization and inlier testing.

Our real data experiment demonstrates the benefit of using our P1AC solvers in place of P3P in an image-based localization pipeline when affine correspondences are available. P1AC achieves pose accuracy comparable to P3P while decreasing the the total computation time.

The downsides we observed when using P1AC instead of P3P were a slight decrease in the number of localized frames on some scenes and a slight increase in average error. Analysis of the frames where P1AC failed but P3P succeeded showed that most of these frames had illumination issues (very dark or strong shadows) or motion blur. These image artifacts likely caused the affine covariant regions to be inaccurately estimated and thus affected the accuracy of the P1AC method.

In comparison to the baseline P3P (1AC) method, which uses point correspondences generated from a single AC, our methods were slightly slower but successfully localized more frames and were more accurate. This indicates that our approach based on differential analysis of the AC more accurately models the constraint imposed by an AC on the absolute pose of the query camera.

There are several approaches to improving the ACs and thus possibly increasing the accuracy of the P1AC result on challenging images. Improving the AC quality might also lead to a speed up in sample consensus because the initial pose estimates by the P1AC solver would be more accurate, and thus the system would spend less time during the local optimization steps. Photometric refinement of the affine transformation is commonly used [41] but is computationally expensive [14]. Barath et al. [3] an efficient alternative called least squares matching (LSM) for symmetric affine correspondence refinement. Eichhardt and Barath introduced a method for multi-view correction of affine frames which could be used to improve the affine frames in the training images but not the query images, since it requires knowledge of the camera pose beforehand [12]. Alternatively, Mischkin et al. introduced a deep learning framework for rapidly detecting high-quality affine regions [37].

With previous minimal solvers that use a single correspondence, histogram or kernel density voting [8] is often used in place of RANSAC. However, we did not find voting to be applicable here because we have a six DOF problem whereas voting is usually applied when estimating a single parameter such as the focal length [17].

## 6 Conclusions and future work

In this work we derived novel constraints imposed by an affine correspondence on the absolute pose of a camera, given knowledge of a 3D point in the scene, the surface normal at that point, and the pose of the reference image. Using these novel constraints we developed two minimal solutions for absolute pose from a single AC. Through experiments on synthetic data we established the numerical stability of our solver and its behavior under increasing levels of noise in the 2D point observation, affine transformation matrix, and normal vector. Finally, we demonstrated the usefulness of our solver in an image-based localization system. In our experiments, replacing P3P with our P1AC solvers decreased computation time while maintaining comparable localization accuracy.

Future work lies in evaluating alternative affine region detectors [37], refinement methods, and sampling strategies [3] to further speed up the localization process and increase reliability. Our work provides a foundation for study of related absolute pose problems with ACs such as handling uncalibrated cameras [7] and radial distortion [20]. The application of ACs to these problems could greatly reduce number of correspondences needed in comparison to approaches based purely on PCs, and would broaden the applicability of the approach to localizing “in-the-wild” images for which camera calibration is not available beforehand.

## References

- [1] Simon Baker and Iain Matthews. Lucas-kanade 20 years on: A unifying framework. *International journal of computer vision*, 56(3):221–255, 2004. 2
- [2] Daniel Barath and Levente Hajder. Novel ways to estimate homography from local affine transformations. In *Proceedings of the International Joint Conference on Computer Vision, Imaging and Computer Graphics Theory and Applications*, pages 434–445, 2016. 7
- [3] Daniel Barath, Michal Polic, Wolfgang Förstner, Torsten Sattler, Tomas Pajdla, and Zuzana Kukelova. Making affine correspondences work in camera geometry computation. In *European Conference on Computer Vision (ECCV)*, 2020. 2, 11, 12
- [4] Connelly Barnes, Eli Shechtman, Adam Finkelstein, and Dan B Goldman. Patchmatch: A randomized correspondence algorithm for structural image editing. *ACM Trans. Graph.*, 28(3):24, 2009. 9
- [5] Adam Baumberg. Reliable feature matching across widely separated views. In *Proceedings IEEE Conference on Computer Vision and Pattern Recognition. CVPR 2000 (Cat. No. PR00662)*, volume 1, pages 774–781. IEEE, 2000. 2
- [6] Jacob Bentolila and Joseph M Francos. Conic epipolar constraints from affine correspondences. *Computer Vision and Image Understanding*, 122:105–114, 2014. 1, 2
- [7] Martin Bujnak, Zuzana Kukelova, and Tomas Pajdla. A general solution to the p4p problem for camera with unknown focal length. In *2008 IEEE Conference on Computer Vision and Pattern Recognition*, pages 1–8. IEEE, 2008. 12
- [8] Martin Bujnak, Zuzana Kukelova, and Tomas Pajdla. Robust focal length estimation by voting in multi-view scene reconstruction. In *Asian Conference on Computer Vision*, pages 13–24. Springer, 2009. 11
- [9] cdcseacave. *OpenMVS: open multi-view stereo reconstruction library*, 2020. 9
- [10] Ondřej Chum, Jiří Matas, and Josef Kittler. Locally optimized ransac. In *Joint Pattern Recognition Symposium*, pages 236–243. Springer, 2003. 1
- [11] Toby Collins and Adrien Bartoli. Infinitesimal plane-based pose estimation. *International journal of computer vision*, 109(3):252–286, 2014. 3
- [12] Ivan Eichhardt and Daniel Barath. Optimal multi-view correction of local affine frames. In *British Machine Vision Conference (BMVC)*, 2019. 11
- [13] Ivan Eichhardt and Daniel Barath. Relative pose from deep learned depth and a single affine correspondence. In *European Conference on Computer Vision*, pages 627–644. Springer, 2020. 2
- [14] Iván Eichhardt and Dmitry Chetverikov. Affine correspondences between central cameras for rapid relative pose estimation. In *Proceedings of the European Conference on Computer Vision (ECCV)*, pages 482–497, 2018. 1, 2, 7, 11
- [15] Martin A Fischler and Robert C Bolles. Random sample consensus: a paradigm for model fitting with applications to image analysis and automated cartography. *Communications of the ACM*, 24(6):381–395, 1981. 1
- [16] J Grunert. Das pothenotische problem in erweiterter gestalt nebst über seine anwendungen in der geodäsie. *Grunerts archive für mathematik und physik*, 1:238–248, 1841. 2
- [17] Levente Hajder and Daniel Barath. Relative planar motion for vehicle-mounted cameras from a single affine correspondence. In *2020 IEEE International Conference on Robotics and Automation (ICRA)*, pages 8651–8657. IEEE, 2020. 11
- [18] Florian Haug and Bernd Jähne. 6 dof appearance-based object localization with local covariant features. *F. Puente León/M. Heizmann (Hrsg.)*, page 13, 2010. 1, 3

- [19] Michal Jancosek and Tomas Pajdla. Exploiting visibility information in surface reconstruction to preserve weakly supported surfaces. *International scholarly research notices*, 2014, 2014. [9](#)
- [20] Klas Josephson and Martin Byrod. Pose estimation with radial distortion and unknown focal length. In *2009 IEEE Conference on Computer Vision and Pattern Recognition*, pages 2419–2426. IEEE, 2009. [12](#)
- [21] Tong Ke and Stergios I Roumeliotis. An efficient algebraic solution to the perspective-three-point problem. In *Proceedings of the IEEE Conference on Computer Vision and Pattern Recognition*, pages 7225–7233, 2017. [3](#)
- [22] Alex Kendall, Matthew Grimes, and Roberto Cipolla. Posenet: A convolutional network for real-time 6-dof camera relocalization. In *Proceedings of the IEEE international conference on computer vision*, pages 2938–2946, 2015. [9](#), [10](#)
- [23] Laurent Kneip, Davide Scaramuzza, and Roland Siegwart. A novel parametrization of the perspective-three-point problem for a direct computation of absolute camera position and orientation. In *CVPR 2011*, pages 2969–2976. IEEE, 2011. [3](#)
- [24] Kevin Köser. *Geometric estimation with local affine frames and free-form surfaces*. PhD thesis, University of Kiel, 2009. [2](#)
- [25] Kevin Köser and Reinhard Koch. Differential spatial resection-pose estimation using a single local image feature. In *European Conference on Computer Vision*, pages 312–325. Springer, 2008. [1](#), [3](#)
- [26] Zuzana Kukelova, Jan Heller, and Andrew Fitzgibbon. Efficient intersection of three quadrics and applications in computer vision. In *Proceedings of the IEEE Conference on Computer Vision and Pattern Recognition*, pages 1799–1808, 2016. [6](#)
- [27] Viktor Larsson. PoseLib - Minimal Solvers for Camera Pose Estimation, 2020. [7](#)
- [28] Viktor Larsson, Kalle Astrom, and Magnus Oskarsson. Efficient solvers for minimal problems by syzygy-based reduction. In *Proceedings of the IEEE Conference on Computer Vision and Pattern Recognition*, pages 820–829, 2017. [5](#)
- [29] Karel Lebeda, Jiri Matas, and Ondrej Chum. Fixing the Locally Optimized RANSAC. In *British Machine Vision Conference (BMVC)*, 2012. [1](#), [10](#)
- [30] Vincent Lepetit, Francesc Moreno-Noguer, and Pascal Fua. Epnnp: An accurate  $o(n)$  solution to the pnp problem. *International journal of computer vision*, 81(2):155, 2009. [10](#)
- [31] Yunpeng Li, Noah Snavely, and Daniel P Huttenlocher. Location recognition using prioritized feature matching. In *European conference on computer vision*, pages 791–804. Springer, 2010. [9](#)
- [32] David G Lowe. Distinctive image features from scale-invariant keypoints. *International journal of computer vision*, 60(2):91–110, 2004. [1](#)
- [33] Bruce D Lucas and Takeo Kanade. An iterative image registration technique with an application to stereo vision. *Proceedings DARPA image Understanding Workshop*, 1981. [2](#)
- [34] Krystian Mikolajczyk and Cordelia Schmid. Scale & affine invariant interest point detectors. *International journal of computer vision*, 60(1):63–86, 2004. [2](#)
- [35] Krystian Mikolajczyk, Tinne Tuytelaars, Cordelia Schmid, Andrew Zisserman, Jiri Matas, Frederik Schaffalitzky, Timor Kadir, and Luc Van Gool. A comparison of affine region detectors. *International journal of computer vision*, 65(1-2):43–72, 2005. [2](#)
- [36] Dmytro Mishkin, Jiri Matas, Michal Perdoch, and Karel Lenc. Wxbs: Wide baseline stereo generalizations. In *Proceedings of the British Machine Vision Conference (BMVC)*, page 12. BMVA Press, 2015. [2](#)
- [37] Dmytro Mishkin, Filip Radenovic, and Jiri Matas. Repeatability is not enough: Learning affine regions via discriminability. In *Proceedings of the European Conference on Computer Vision (ECCV)*, pages 284–300, 2018. [2](#), [11](#), [12](#)
- [38] David Nistér. An efficient solution to the five-point relative pose problem. *IEEE transactions on pattern analysis and machine intelligence*, 26(6):756–770, 2004. [2](#)
- [39] David Nister and Henrik Stewenius. Scalable recognition with a vocabulary tree. In *2006 IEEE Computer Society Conference on Computer Vision and Pattern Recognition (CVPR'06)*, volume 2, pages 2161–2168. Ieee, 2006. [10](#)
- [40] Mikael Persson and Klas Nordberg. Lambda Twist: An accurate fast robust perspective three point (p3p) solver. In *Proceedings of the European Conference on Computer Vision (ECCV)*, pages 318–332, 2018. [1](#), [3](#), [6](#), [8](#)



- [41] Carolina Raposo and Joao P Barreto. Theory and practice of structure-from-motion using affine correspondences. In *Proceedings of the IEEE Conference on Computer Vision and Pattern Recognition*, pages 5470–5478, 2016. 1, 2, 11
- [42] Torsten Sattler et al. RansacLib - A Template-based \*SAC Implementation, 2019. 10
- [43] Johannes Lutz Schönberger and Jan-Michael Frahm. Structure-from-motion revisited. In *Conference on Computer Vision and Pattern Recognition (CVPR)*, 2016. 9
- [44] Johannes Lutz Schönberger, True Price, Torsten Sattler, Jan-Michael Frahm, and Marc Pollefeys. A vote-and-verify strategy for fast spatial verification in image retrieval. In *Asian Conference on Computer Vision (ACCV)*, 2016. 10
- [45] Johannes Lutz Schönberger, Enliang Zheng, Marc Pollefeys, and Jan-Michael Frahm. Pixelwise view selection for unstructured multi-view stereo. In *European Conference on Computer Vision (ECCV)*, 2016. 9
- [46] A. Vedaldi and B. Fulkerson. VLFeat: An open and portable library of computer vision algorithms. <http://www.vlfeat.org/>, 2008. 9
- [47] Jonathan Ventura, Clemens Arth, Gerhard Reitmayr, and Dieter Schmalstieg. A minimal solution to the generalized pose-and-scale problem. In *Proceedings of the IEEE Conference on Computer Vision and Pattern Recognition*, pages 422–429, 2014. 5
- [48] Changchang Wu. Towards linear-time incremental structure from motion. In *2013 International Conference on 3D Vision-3DV 2013*, pages 127–134. IEEE, 2013. 9
- [49] Changchang Wu, Sameer Agarwal, Brian Curless, and Steven M Seitz. Multicore bundle adjustment. In *CVPR 2011*, pages 3057–3064. IEEE, 2011. 9
- [50] Lipu Zhou, Jiamin Ye, and Michael Kaess. A stable algebraic camera pose estimation for minimal configurations of 2d/3d point and line correspondences. In *Asian Conference on Computer Vision*, pages 273–288. Springer, 2018. 6